Journal of Renewable Materials

Tech Science Press

DOI: 10.32604/jrm.2022.023266

check for updates

ARTICLE

Characteristic of Fresh and Harden Properties of Polyvinyl Alcohol Fibre Reinforced Alkali Activated Composite

Yiguang Wang[1,2], Zhe Zhang[1] and Xun Zhang[1,*]

[1]School of Civil Engineering, Zhengzhou University, Zhengzhou, 450001, China

[2]Henan Provincial Communications Planning, Survey & Design Institute Co., Ltd., Zhengzhou, 450001, China

[*]Corresponding Author: Xun Zhang. Email: Zhangxun@zzu.edu.cn

Received: 17 April 2022 Accepted: 20 June 2022

ABSTRACT

Fibre can enhance the mechanical properties of cement-based composites, but fibre also degrades their workability. However, the quantitative effects of fiber content and length-diameter ratio on alkali-activated materials are still unclear. Various aspect ratio, volume fraction of polyvinyl alcohol fibre (PVAF), and various water-binder ratio were employed to prepare a total of 26 groups of fibre reinforced alkali-activated composite (FRAAC). The influence of PVAF fibre factor (product of fiber volume fraction and length-diameter ratio) on flowability, compactness, strength, and crack fractal dimension of FRAAC was researched. The influence of water-binder ratio on the plastic viscosity of FRAAC was more significant than that on the yield stress. When fibre factor was lower than critical value of 150, the influence of fibres could be overlooked. The reason was that the space between fibres was distant, so the flowability of FRAAC was not impacted by PVAF. At this time, fibres were challenging to restrict the cracks in matrix and increase their mechanical properties. When fibre factor was higher than critical value 150 and lower than density packing value 450, the flexural strength, compressive strength and crack fractal dimension of FRAAC were considerably enhanced, and the FRAAC could still flow easily under dead weight. When fibre factor were above 450, noteworthy fibre balling considerably decreased the flowability, leading to poor solidity and reduced compressive strength. Hence, the ideal content of PVAF in alkali activated composite is between 150/(l/d) and 450/(l/d).

KEYWORDS

Alkali-activated composite; fibre reinforced composite; fibre factor; flowability; strength; fractal dimension

Nomenclature

FF	Fiber factor
l/d	Length to diameter ratio
F_c	Critical fiber factor
F_d	Dense fiber factor

1 Introduction

Alkali activated composite is a green, low emission, and low energy consumption substitute of Portland cement. Alkali activated composite can absorb a large amount of solid waste and presents environmental

protection, economic and social benefits [1–4]. Compared with Portland cement-based materials, alkali-activated materials have more brittleness. Introducing fibre is one of the effective methods to improve the tensile strength and toughness of alkali-activated materials [5]. Because the reaction mechanism and raw material composition are fundamentally different from traditional Portland cement based materials, there are obvious differences between the flowability of alkali-activated materials and cement-based materials. For example, Criado et al. [6] revealed that the plastic viscosity of alkali activated fly ash paste was significantly higher than that of Portland cement paste, but its yield stress is mostly lower than that of Portland cement paste. Guo [7] indicated that conventional water reducing agent could not improve the flowability of alkali-activated slag-silica fume high-strength mortar. But water reducing agent caused its strength to decrease after hardening. These differences will also have a significant impact on the physical and mechanical properties of alkali-activated materials after hardening. Therefore, it is necessary to carry out a systematic study on the flowability as well as physical and mechanical properties of alkali-activated materials.

Due to the brittle nature of concrete, various fibres are introduced to overcome this shortcoming [1–3,8–32]. While the brittleness of alkali-activated concrete is higher than Portland cement concrete. The application of steel fibre [33–37], polypropylene fibre [38–40], polyvinyl alcohol fibre (PVAF) [41–44] and hybrid fibres [8,45–57] in cement-based materials and alkali-activated materials are the most widely studied topic [58,59]. Among them, PVAF has become one of the most widely used fibre in cement-based materials and alkali-activated materials due to its significant advantages of low cost, high chemical stability and easy construction [43,60–62]. The international market prices of PVA fibre and steel fibre are 1–15 and 1–8 $/kg, respectively. If the PVAF with lower density is mixed in the same volume, its cost advantage is more prominent compared with steel fibre [59]. Therefore, PVAF has been used to prepare PVAF reinforced alkali activated mortar (PFRAAC) in this paper.

High content and aspect ratio (the ratio of length to diameter) of the fibre can enhance the hardened property of fiber reinforced cementitious composites significantly [63]. Unfortunately, fibers degrade the workability of fresh cementitious composites. Swamy et al. [64] indicated the existence of a critical content of fibres above which the cementitious composite could not flow under the action of self-weight, even when the fibers were in large fluidity cementitious composite. Both fiber content and aspect ratio have significant effects on the workability and mechanical properties of cement-based composites. Hence, the fibre factor (FF, namely the product of fibre volume fraction and fibre aspect ratio) is proposed to assess the working and mechanical properties of fibre cement matrix composites. For example, Said et al. [43,65] pointed out that the flexural deflection, toughness and tensile strength of strain-hardened cement-based composites increased linearly with FF of PE fibre and PVAF. Cao et al. [28] found that the flowability and flexural toughness of hybrid fibre reinforced cement-based composites had a quadratic function relationship with FF. Mehdipour et al. [66] studied the flowability, volume stability and mechanical properties of glass fibre self-compacting mortar and found that the optimal FF of glass fibre in self-compacting mortar was about 450. The optimal FF of polypropylene fibre in mortar is between 100 and 300 [67].

However, the effect of PVAF FF on the fresh-mixing properties and hardened properties of alkali-activated materials is unclear. Moreover, the difference between PVAF and traditional fibre in cement and alkali-activated based composites is unknown. Therefore, a total of 26 groups of FRAAC were prepared by using two different fibre aspect ratio, six different volume dosages, and two water-binder ratios, in order to study the influence of FF on slump flow, V-funnel flow velocity, apparent density, ultrasonic wave velocity, compressive strength, bending strength, bending to compressive strength ratio, and fractal dimension of cracks. The FF thresholds for loose and tight packing are determined and the differences between FRAAC and conventional fibre-reinforced cement-based composites are discussed.

2 Experimental Materials and Methods

2.1 Raw Material

Mineral admixtures used in this study included secondary fly ash (Hebei Kesu Building Materials Co., Ltd., China), S95 granulated blast furnace slag powder (Tianjin Yandong Mineral Products Co., Ltd., China) and silica fume (Gansu Sanyuan Silicon Materials Co., Ltd., China). The composition of oxides of raw materials is shown in Table 1. The particle size distribution curves of the mineral admixtures are presented in Fig. 1. The activator includes sodium silicate solution (Jinan Mingchuan Chemical Co., Ltd., China, mass fraction of Na_2O and SiO_2 are 9.0% and 28.08% respectively, modulus was 3.22) and sodium hydroxide (Cangzhou Shengqiang Chemical Products Co., Ltd. (China), purity is above 96%). The water was municipal tap water. PVAF was produced by Anhui Wanwei Co., Ltd., China with 6 mm and 12 mm length, 40 μm diameter, 1500 MPa tensile strength, 36.7 GPa elastic modulus and density of 1.29 g/cm^3.

Table 1: Composition of oxides of raw materials as wt.%

Composition	SiO_2	CaO	Al_2O_3	Fe_2O_3	MgO	K_2O	SO_3	Na_2O
Fly ash	51.50	9.79	24.36	5.49	1.20	1.04	2.14	0.51
Slag	27.89	33.12	15.57	0.36	0.30	0.44	1.10	0.49
Silica fume	93.50	0.78	0.16	0.10	0.95	2.89	0.84	0.23

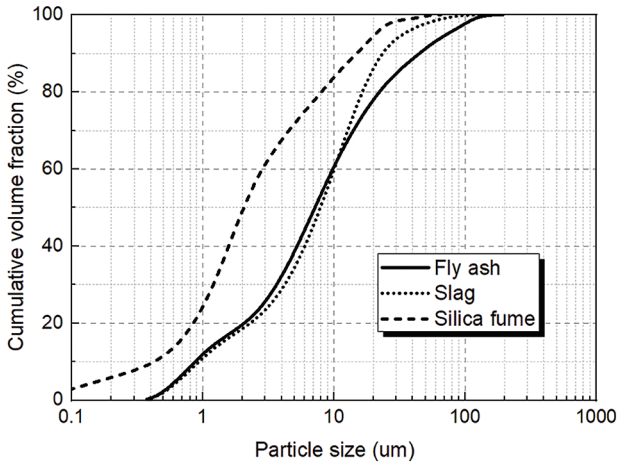

Figure 1: Size distribution of mineral admixtures

2.2 Mix Ratio and Mixing Process

Water-binder ratio was set as 0.44 and 0.47. The mass ratio of fly ash: slag: silica fume was set as 1:0.14:0.29. Fixed sand-binder ratio was 0.5. PVAF of 6 and 12 mm length was added, and the fibre volume dosage was 0.0%, 0.3%, 0.6%, 1.0%, 1.5%, 2.0% and 2.5%, respectively. 26 groups of FRAAC proportions with different fibre factors and water-binder ratios were obtained, as shown in Table 2. Cement mortar mixer was used for mixing FRAAC. The mixing process is shown in Fig. 2.

After flowability test, the mixed FRAAC was poured into the mold and vibrated. Then the specimen was covered with plastic film. The mold was removed 24 h later, and cured in a standard curing chamber with standard temperature and humidity (20 ± 2°C, relative humidity ≥95%) for 28 days.

Table 2: Mixture proportion of FRAAC

Specimen No. (*X-Y-Z*)*	Water-binder ratio	Fibre volume of PVAF/%	Aspect ratio	Fibre factor
0.44-0	0.44	0.0	150	0
0.44-6-0.3	0.44	0.3	150	45
0.44-6-0.6	0.44	0.6	150	90
0.44-6-1.0	0.44	1.0	150	150
0.44-6-1.5	0.44	1.5	150	225
0.44-6-2.0	0.44	2.0	150	300
0.44-6-2.5	0.44	2.5	150	375
0.44-12-0.3	0.44	0.3	300	90
0.44-12-0.6	0.44	0.6	300	180
0.44-12-1.0	0.44	1.0	300	300
0.44-12-1.5	0.44	1.5	300	450
0.44-12-2.0	0.44	2.0	300	600
0.44-12-2.5	0.44	2.5	300	750
0.47-0	0.47	0.0	150	0
0.47-6-0.3	0.47	0.3	150	45
0.47-6-0.6	0.47	0.6	150	90
0.47-6-1.0	0.47	1.0	150	150
0.47-6-1.5	0.47	1.5	150	225
0.47-6-2.0	0.47	2.0	150	300
0.47-6-2.5	0.47	2.5	150	375
0.47-12-0.3	0.47	0.3	300	90
0.47-12-0.6	0.47	0.6	300	180
0.47-12-1.0	0.47	1.0	300	300
0.47-12-1.5	0.47	1.5	300	450
0.47-12-2.0	0.47	2.0	300	600
0.44-12-2.5	0.47	2.5	300	750

Note: *: *X* represents water-binder ratio, *Y* represents fibre length, *Z* represents fibre volume fraction.

Figure 2: Mixing procedure of FRAAC

2.3 Flowability Test of Fresh Mortar

A small V-shaped funnel was used to measure the flow velocity (FV) of the FRAAC. The V-funnel FV was calculated as the volume of the V-shaped funnel (1134 mL) divided by the flow time (measured in s) from the opening of the lower port switch to the light being seen through the lower port. A small slump

cylinder was used to measure the slump flow (SF) of FRAAC. The instrument size and experimental method used for flowability test can be referred to as references [32,68].

2.4 Compactness Test of Hardened Mortar

The mass of three specimens in each group was measured, and the apparent density (AD) of the specimen was derived from the ratio of mass to volume. The velocity of ultrasonic pulse (UPV) wave propagation in FRAAC was measured using a non-metallic ultrasonic analyzer manufactured by Earth Products China Co., Ltd. (China) in accordance with ASTM C597 [69].

2.5 Mechanical Properties Test of Hardened Mortar

The flexural strength (f_f) and compressive strength (f_c) of FRAAC were tested in accordance with GB/T 17671 [70]. After FRAAC's flexural strength test, digital camera was used to collect the surface crack morphology of specimens after bending failure, and IMAGE PRO was used to extract cracks. The method was referenced [56], and the fractal dimension (FD) of cracks was calculated.

3 Results and Discussion

3.1 The Impact of FF on FRAAC Flowability

For theoretical analysis a fibre factor (FF), defined as the product of fibre volume and aspect ratio (length/diameter ratio), has been recommended to predict the workability and mechanical properties of fibre reinforced cementitious composites [66,67,71]. One motive for using FF was that it has noteworthy influence on the packing density of the fibre-particle system in fibre reinforced cementitious composites [21].

Fig. 3 shows the relationship between relative V-funnel FV and relative SF of FRAAC and FF at water-binder ratios of 0.44 and 0.47. The FV and SF of FRAAC decreased significantly with increasing FF, but the rate of decline gradually decreased and stabilized with increasing FF. According to Krieger and Dougherty's theory [72] and Philipse's random contact equation [73], fibre reinforced cement-based composites could be simplified as rigid spherical particles and rods suspended in slurry. Based on the value of FF, the flowability index of fibre reinforced cement matrix composites could be divided into three stages [66,67,71]. Similarly, FRAAC's V-funnel FV and SF could be divided into three zones:

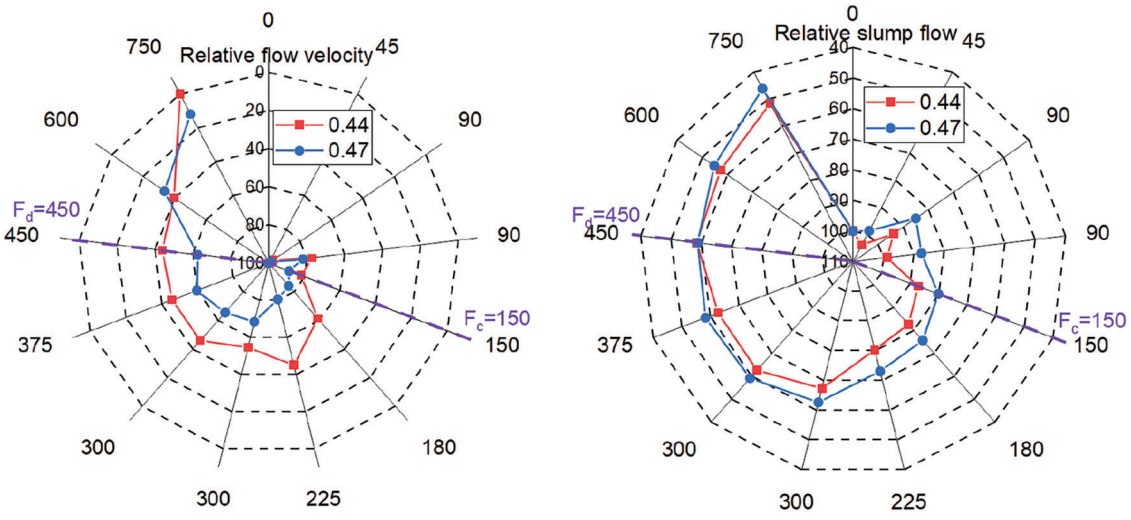

(a) Relative V-funnel flow velocity (b) Relative slump flow

Figure 3: Relationships of (a) FF–V-funnel flow velocity and (b) FF–slump flow of FRAAC

In the first stage, FF < Fc = 150, FRAAC was dilute suspension, and fibre had little influence on the fluidity of mortar. The relative V-funnel FV and relative SF of FRAAC were both higher than 80% of control group without PVAF. At this stage, the fibres were far enough apart to ignore fibre interactions. As a result, the fluidity of FRAAC was essentially the same as that of fibre-free mortar. The SF of FRAAC with a water-binder ratio of 0.44 was slightly higher than that of the control group, presenting a relative SF higher than 100%, as shown in Fig. 3b. When the mortar flowed, the fibre dispersion was good, and there was no fibre lap agglomeration phenomenon.

In the second stage, $F_c = 150 < FF < F_d = 450$, the contact between fibres increased and began to affect the fluidity of mortar. For FRAAC with a water-binder ratio of 0.44, the increase in FF from 0 to 150 and 375 resulted in a reduction in SF of approximately 10% and 40%, respectively. As shown in Fig. 3, increasing FF significantly reduced the V-funnel FV and SF of FRAAC at stage 2. The relative V-funnel FV was between 80% and 40% of control group without PVAF. The relative SF was between 80% and 60% of control group without PVAF. As FF increased near $F_d = 450$, FRAAC workability was controlled by contact and collision of fibers. Experimental phenomenon at stages 1 and 2 showed that the fibres were evenly dispersed without significant instability or clumps, and the FRAAC remained fluid enough to flow freely under its own weight.

In stage 3, $FF > F_d = 450$, FRAAC's liquidity deteriorated rapidly and was no longer free flowing. The relative V-funnel FV and relative SF of FRAAC was lower than 40% and 60% of control group without PVAF. Fibres were poorly dispersed and showed significant clumps, which greatly reduced the fluidity and stability of the FRAAC. According to Krieger and Dougherty's theory, FRAAC's fibre volume fraction at this stage approached the upper limit of random compact packing. In this case, improving the fluidity of FRAAC by simply increasing the water-binder ratio might result in significant segregation and bleeding, which severely degraded the workability of the mortar. Whether the water-binder ratio was 0.44 or 0.47, when FF increased from 0 to 750, the SF decreased by about 50%, while the FV decreased by 100%. The FV was more sensitive than SF to the change of FF. The SF and FV of FRAAC with a water-binder ratio of 0.47 were higher than those of FRAAC with a water-binder ratio of 0.44, but the difference in FV was also larger than that of FRAAC with a water-binder ratio of 0.44. This indicated that FV was also more sensitive to changes in water-binder ratio. That was to say, the effect of fibre/water-binder ratio on the plastic viscosity of FRAAC was more significant than the effect of yield stress. Similarly, Mehdipour et al. [66] also showed that the workability of glass fibre cement mortar measured by SF was not as stable as the V-funnel FV. This is because SF evaluated the free deformation capacity of mortar, but SF could not reflect the deformation capacity of mortar under constraints, especially in fibre reinforced cement-based materials.

Fig. 4 shows the comparison of relative SF of fibre reinforced mortar between this paper and literatures [66]. In literature [66] and [67], except for the fibers, all other parameters *i.e.* the water to cement ratio (w/c = 35%) and the superplasticizer dosage (0.5% of cement mass) were kept constant in all mixtures. No matter the water-binder ratio was 0.44 or 0.47, the relative SF of PVAF alkali activated mortar was lower than that of PP fibre cement mortar but higher than that of glass fibre cement mortar at FF ≈ 300 and 700. That was, PVAF degraded the workability of alkali activated mortar more significantly than PP fibre degraded the workability of cement mortar, which was weaker than glass fibre degraded the workability of cement mortar. This is because the greater the friction between the fibres, the more energy is required for the fibre reinforced mortar to achieve the same workability [67]. The amount of friction between fibres is proportional to the normal force between the fibres in contact, which is a function of fibre stiffness. According to the theory of Martinie et al. [74], the stiffness index of fibre is defined as Eq. (1).

$$\frac{f}{l} \cong \frac{\tau_0}{E}(l/d)^3 \tag{1}$$

where, τ_0 is the yield stress of cement-based material, E is the elastic modulus of fibre, and l/d is the length-diameter ratio of fibre. The rigidity index of PVAF used in this paper was less than 1% [74]. The stiffness

indices of steel fibre, glass fibre and PP fibre in Portland cement-based composites in literature were 0.03%, 2% and 39-3500%, respectively [24]. The stiffness index PVAF of FRAAC in this paper was between 55%–931% and higher than 1%. As a typical flexible fibre, its value was between PP fibre and glass fibre in Portland cement mortar.

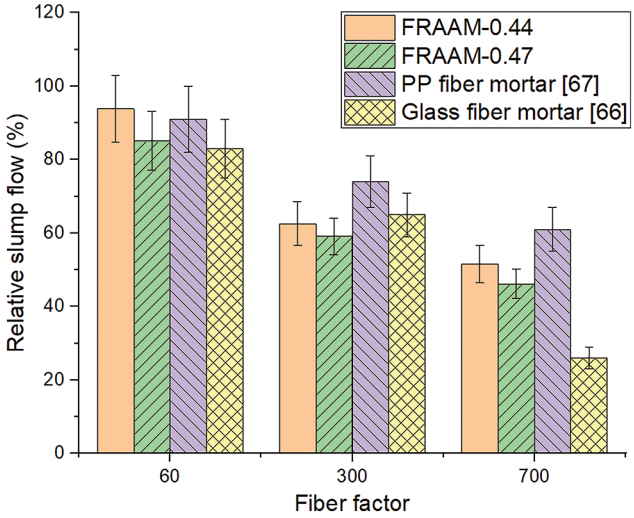

Figure 4: Comparison of relative flow spread of fibre reinforced mortar of this paper and literature [66,67]

3.2 Effect of FF on FRAAC Apparent Density and Ultrasonic Wave Velocity

Fig. 5 shows the relationship between apparent density and FF. The apparent density of FRAAC with w/b of 0.44 was higher than that of 0.47, and the data discretization of FRAAC with water-binder ratio of 0.47 was greater. The decrease of apparent density was caused by the increase of free water in alkali-activated mortar, and the serious bleeding of water-binder ratio group also led to the deterioration of the stability of the mixture. The results of apparent density after hardening were more discrete.

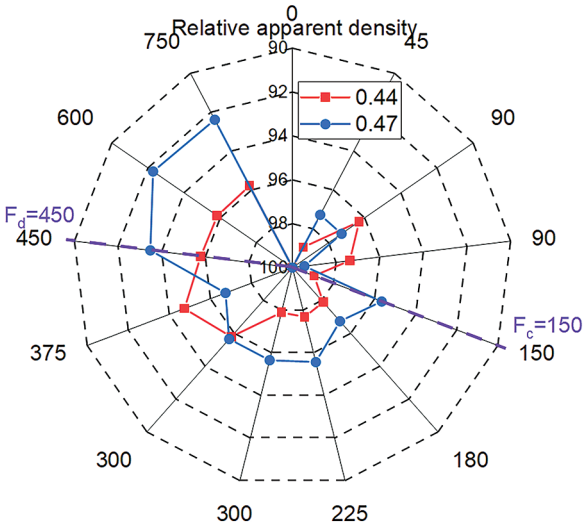

Figure 5: Relationships of FF–apparent density of FRAAC

With the increase of FF, the overall apparent density decreased. The apparent density was a measure of the density and uniformity of FRAAC. During stage 1 and stage 2 (FF < 450), the apparent density decreased at a lower rate. The workability of FRAAC was generally good, with no obvious fibrous clumping, resulting in a denser FRAAC with a higher apparent density. At the third stage (FF > 450), the apparent density was decreased significantly with the increase of FF, which was caused by fibre clumping and uneven dispersion.

The test results of ultrasonic wave velocity also confirmed the above analysis, as shown in Fig. 6. When the water-binder ratio was 0.44, with the increase of FF, the ultrasonic wave velocity showed a trend of increasing first and then decreasing, and reached the peak at the second stage (150 < FF < 450). Ultrasonic wave velocity reflected the density and uniformity of mortar. During the first and second stages (FF < 450), the apparent density of FRAAC was relatively high. The PP fibres bridged the defects and initial cracks that facilitated ultrasonic transmission, thus increasing the ultrasonic wave velocity of FRAAC [29]. In the third stage (FF > 450), the ultrasonic wave velocity decreased significantly with the increase of FF. This resulted from the decrease of the apparent density of the matrix, and the uneven fibre agglomeration and dispersion also reduced the ability to bridge defects and initial cracks. Similar to the apparent density results, the ultrasonic wave velocity results of the high water-binder ratio group were also more discrete.

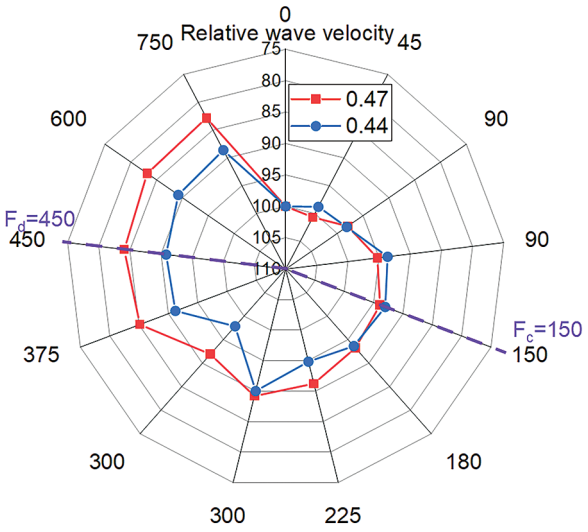

Figure 6: Relationships of FF–ultrasonic velocity of FRAAC

3.3 Effect of FF on FRAAC Strength

The effect of FF on the flexural strength of FRAAC is shown in Fig. 7. The addition of PVAF significantly improved the flexural strength of alkali-activated mortar. The PVAF bridged cracks to transfer loads, limiting the development of cracks. In general, the FRAAC's flexural strength was increased with the increase in FF because both the number of fibres and the length of the fibres increased its ability to bridge cracks. For FRAAC with a water-binder ratio of 0.44, the flexural strength began to decrease significantly when FF > 450. When FF > 450, the flexural strength of FRAAC with a water-binder ratio of 0.47 was higher than that of FRAAC with a water-binder ratio of 0.44. This indicated that the improvement of tensile strength of mortar by fibre was more significant than the deterioration caused by internal defects of matrix.

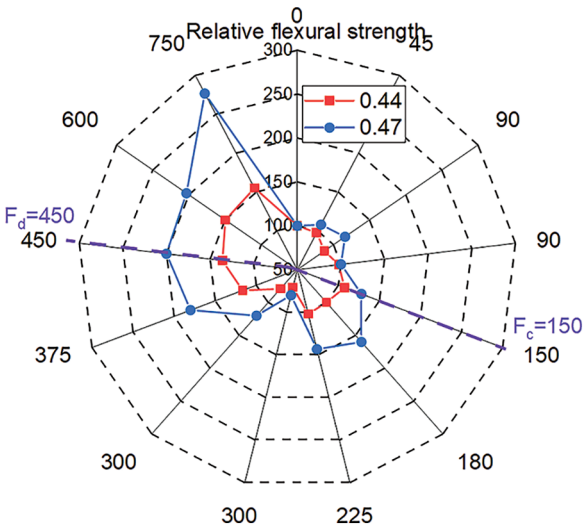

Figure 7: Relationships of FF–bending strength of FRAAC

Fig. 8 shows the comparison of flexural strength between fibre reinforced mortars in this paper and those in literature. When FF was about 60 and 300, the flexural strength of PVAF alkAli, Mortar was lower than that of PVAF cement mortar and glass fibre cement mortar. However, when FF was about 700, the flexural strength of PVAF alkAli, Mortar was higher than that of PVAF cement mortar and glass fibre cement mortar. The main reason was that the plastic viscosity of alkali-activated materials was significantly higher than that of Portland cement based materials [6]. The distribution and orientation of PVAF in alkali-activated mortar with 0.44 w/b ratio were worse than that in cement mortar, so the flexural strength of PVAF alkali-activated mortar was generally lower than that of PVAF cement mortar. However, when the water-binder ratio was large, the plastic viscosity of the matrix decreased. The distribution and orientation of PVAF were improved, so the flexural strength of PVAF alkali-activated mortar with 0.47 w/b ratio was significantly increased. When the fiber factor reached 700, the fibers in low w/b ratio mortar were easy to cluster, while the PVAF alkali-activated mortar with 0.47 w/b ratio was more suitable for good fiber dispersion. Hence, the FRAAM-0.47 reached the highest value of relative bending strength, shown in Fig. 8.

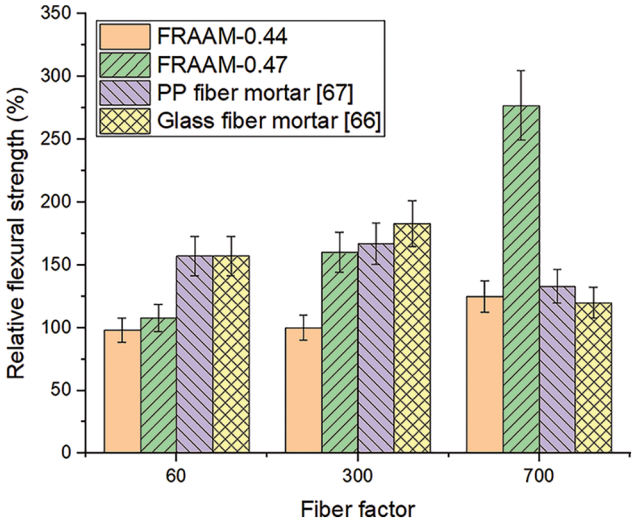

Figure 8: Comparison of relative bending strength of fibre reinforced mortar between this paper and literatures

Fig. 9 shows the influence of FF on compressive strength. The specific compressive strength is presented in Table 3. The compressive strength was increased firstly (more than 6%). But when FF reaches about 450, the compressive strength began to decline, which was close to the variation trend of ultrasonic wave velocity. The reason was that when FF was less than 450, the fibre was generally well dispersed without obvious agglomeration, and the fibre improved the energy dissipation capacity of mortar, as well as compressive strength, flexural strength and ultrasonic wave velocity. However, when FF exceeded F_d = 450, fibres tended to show significant clumping, resulting in more defects in mortar, which reduced the compressive strength, apparent density and ultrasonic wave velocity of mortar. By comparing Figs. 7 and 9, it could be found that when FF = 450 or so, the decreasing trend of compressive strength was more obvious than that of flexural strength, because the compressive strength was more sensitive to the defects in the mortar.

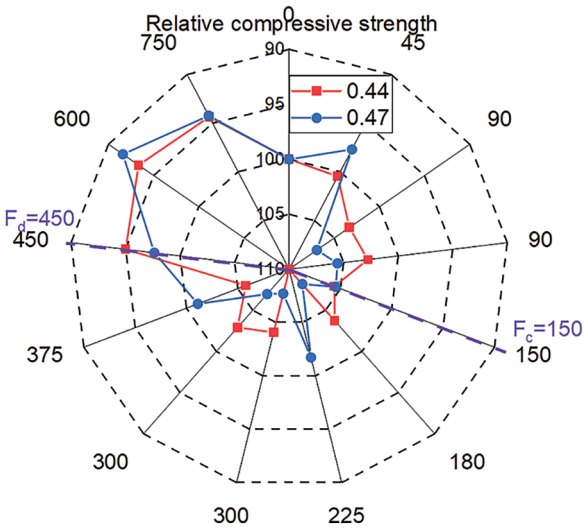

Figure 9: Relationships of FF–compressive strength of FRAAC

Table 3: Compressive strength of FRAAC

Fiber factor	Compressive strength/MPa (w/b = 0.47)	Compressive strength/MPa (w/b = 0.44)
0	22.1	24.5
45	22.20231	23.93412
90	22.94239	25.59255
90	23.57968	27.01659
150	24.90058	28.49152
180	25.83435	30.82468
225	28.40582	31.35865
300	29.5631	33.77845
300	30.42535	36.13674
375	32.18608	36.5351
450	30.57678	35.67206
600	28.53832	32.67599
750	26.92644	30.78918

Fig. 10 shows the comparison of compressive strength of fibre reinforced mortars in this paper and literatures [66,67]. When FF was about 60, 300 and 700, the compressive strength of PVAF alkali activated mortar was greater than that of PVAF cement mortar and glass fibre cement mortar. That was, PVAF had a relatively small deterioration effect on the compressive strength of alkali-activated mortar, and even improved compressive strength to a certain extent. While PVAF and glass fibre had a more significant deterioration effect on cement mortar. The reason was that the interface bond between fiber and matrix in alkali activated mortar was stronger than that in cement mortar [75]. Shi et al. [76] believed that the interfacial transition zone of alkali-activated materials was more dense and uniform due to the water reducing effect of Na_2SiO_3 in pore solution and the higher initial concentration of $(SiO_4)^{-4}$.

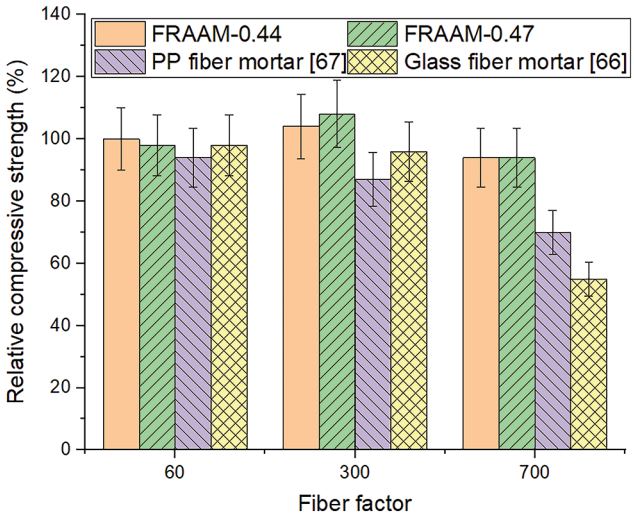

Figure 10: Comparison of relative compressive strength of fibre reinforced mortar between this paper and literatures

Fig. 11 shows the effect of FF on FRAAC and fibre-reinforced cement mortars. The flexural to compressive strength ratio was often used to measure the toughness of cement-based materials. The higher the flexural to compressive strength ratio, the higher the toughness of cement-based materials [77]. When FF < 150, there was no significant difference between FRAAC and fibre-reinforced cement mortar in the flexural to compressive strength ratio. The flexural to compressive strength ratio of some FRAAC specimens was slightly lower than that of fibre-reinforced cement mortar. The reason was that the number of fibre at this stage was relatively small, which made it difficult to fully use its cracking resistance and toughening effect. The strength and toughness of specimens were mainly controlled by the matrix. Ding et al. [78] confirmed that the brittleness of alkali-activated materials without fibre was higher than that of cement-based materials. With the increase of FF, the flexural to compressive strength ratio of FRAAC was increased faster than that of fibre reinforced cement mortar. When FF > 150, PVAF toughened alkali activated mortar better than cement mortar. When FF > 450, FRAAC with a water-binder ratio of 0.44 and 0.47 had a greater flexural ratio than fibre-reinforced cement mortar with the same FF ratio, indicating that FRAAC was more ductile than fibre-reinforced cement mortar with the same FF ratio. This was due to better interfacial bonding between PVAF and alkali activated mortar [75]. This dissipated more energy when pulling out and breaking, and thus FRAAC had better toughness than fibre-reinforced cement mortar.

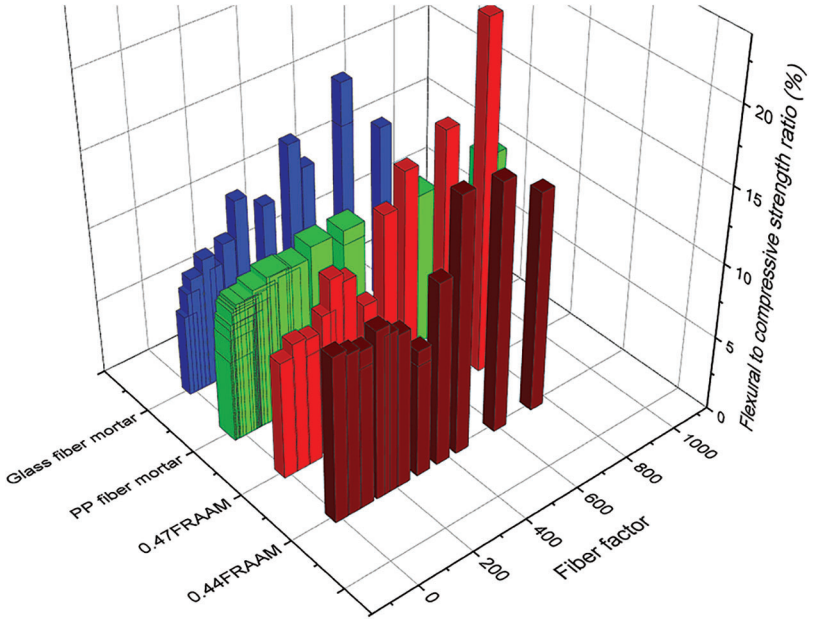

Figure 11: Relationships of FF–flexural to compressive strength ratio of fibre reinforced mortar [66,67]

3.4 Influence of FF on FRAAC Crack Characteristics

As FF increased, the crack morphology of the FRAAC under flexural failure also changed significantly, in addition to the increased flexural strength. In general, high toughness concrete is usually accompanied by multiple cracking failure mode. With the increase of RI, the crack morphology changes from single crack to multi-crack cracking pattern, corresponding to the high toughness of concrete. In order to quantitatively evaluate the influence of FF on crack characteristics during FRAAC failure, the images of cracks on the side and bottom of the specimen were captured by digital camera firstly. Subsequently, the captured crack images were processed and edited with software of IMAGE PRO to get a clear crack profile using binarizing, thresholding, cleaning and filtering methods [79]. Fractal dimension could be used to describe the complexity of concrete crack morphology, and box-counting dimension method was used to describe the fractal characteristics of cracks quantitatively. Box-counting dimension method was a calculation method for measuring fractal dimension of space. The crack binary image was placed on an evenly divided box and the minimum number of boxes needed to completely cover the crack was calculated. The box size was reduced step by step, the change in the required number of boxes was recorded [3]. Assuming that the box side length is a, the space was divided into N boxes, and the fractal dimension was defined as follows:

$$Fractal_{box}(\text{crack}) = \lim_{\text{a}\to 0} \frac{\log N(\text{a})}{\log N(1/\text{a})} \tag{2}$$

The change of fractal dimension of FRAAC surface crack with FF is shown in Fig. 12. With the increase of the FF, FRAAC surface crack fractal dimension overall showed a trend of increase. The reason was that with the increase of quantity and length of fibre, fibre bridged crack efficiency. This increased the twists, turns and number of cracks. The cracks became more complicated and its fractal dimension was increased.

In general, the crack fractal dimension of FRAAC with a water-binder ratio of 0.44 was larger than that of FRAAC with a water-binder ratio of 0.47 at the stage FF < 450. At the stage of FF > 450, the crack fractal dimension of FRAAC with a water-binder ratio of 0.44 was smaller than that of FRAAC with a water-binder ratio of 0.47. This was similar to the variation rule of flexural strength in Fig. 7, indicating that the fractal

dimension of cracks had a certain correlation with its flexural strength [34]. In addition, the changing rule of fracture fractal dimension also confirmed that the introduction of PPF could significantly improve the toughness of alkali-activated mortar.

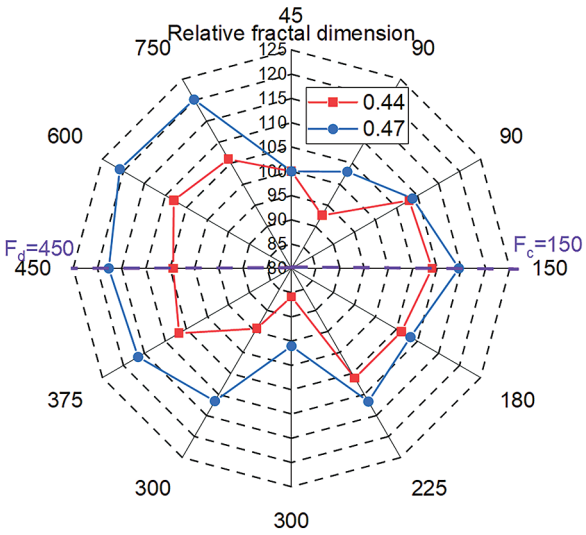

Figure 12: Relationships of FF–Cracks fractal dimension of FRAAC

4 Conclusion

(1) The fibre factor and water-binder ratio had a more significant effect on the flow rate than on the slump spread of alkali-activated mortar. This indicated that the influence of fibre and water-binder ratio on the plastic viscosity was greater than that on the yield stress of alkali-activated mortar.

(2) When FF was less than $F_c = 150$, the influence of fibre could be ignored. The distance between fibres was far, and the workability of mortar was basically not affected. There was little difference in reinforcing effect of PVAF, polypropylene fibre and glass fibre on workability and mechanical properties of alkali activated mortar and cement mortar.

(3) When FF value was between $F_c = 150$ and $F_d = 450$, the flexural strength, compressive strength, flexural to compressive strength ratio and fractal dimension of cracks of alkali-activated mortar were significantly improved. PVAF had a better reinforcing effect on mechanical properties of alkali-activated mortar than that of cement mortar by polypropylene fibre and glass fibre.

(4) When FF value was higher than $F_d = 450$, significant fibre balling greatly deteriorated the workability of alkali activated mortar. The compactness and compressive strength of hardened mortar became worse. PVAF FRAAC with 0.47 w/b presented much higher flexural strength, flexural to compressive strength ratio and fractal dimension ratio than that of polypropylene fibre and glass fibre reinforced cement mortar.

(5) The thresholds of PVAF reinforced alkali-activated mortar in loose and close stacking states were 150 and 450, respectively. The optimal volume content of PVAF in alkali-activated mortar was between 150/(l/d) and 450/(l/d).

Acknowledgement: The authors acknowledge the financial support provided by the following funds.

Funding Statement: The authors received funding of Henan Province Transportation Science and Technology Plan Project (2021J3).

Conflicts of Interest: The authors declare that they have no conflicts of interest to report regarding the present study.

References

1. Zhang, N., Yan, C., Li, L., Khan, M. (2022). Assessment of fiber factor for the fracture toughness of polyethylene fiber reinforced geopolymer. *Construction and Building Materials, 319,* 126130. DOI 10.1016/j.conbuildmat.2021.126130.
2. Hu, C., Li, L., Li, Z. (2022). Effect of fiber factor on the workability and mechanical properties of polyethylene fiber-reinforced high toughness geopolymers. *Ceramics International, 48(8),* 10458–10471.
3. Li, L., Sun, H., Zhang, Y., Yu, B. (2021). Surface cracking and fractal characteristics of bending fractured polypropylene fiber-reinforced geopolymer mortar. *Fractal and Fractional, 5(4),* 142. DOI 10.3390/fractalfract5040142.
4. Li, L., Wei, Y., Li, Z., Farooqi, M. U. (2022). Rheological and viscoelastic characterizations of fly ash/slag/silica fume-based geopolymer. *Journal of Cleaner Production, 354,* 131629. DOI 10.1016/j.jclepro.2022.131629.
5. Silva, G., Kim, S., Aguilar, R., Nakamatsu, J. (2020). Natural fibers as reinforcement additives for geopolymers–A review of potential eco-friendly applications to the construction industry. *Sustainable Materials and Technologies, 23,* e00132. DOI 10.1016/j.susmat.2019.e00132.
6. Criado, M., Palomo, A., Fernández-Jiménez, A., Banfill, P. F. G. (2009). Alkali activated fly ash: Effect of admixtures on paste rheology. *Rheologica Acta, 48(4),* 447–455. DOI 10.1007/s00397-008-0345-5.
7. Guo, J. (2017). *Research on process and properties of alkali-activated cement based ultra-high performance concrete (Master Thesis)*. Fuzhou University, China.
8. Li, L., Xie, C., Cao, M., Zhou, X., Li, Z. (2022). Synergistic effect between $CaCO_3$ Whisker and Steel-PVA fiber cocktail in cement-based material at elevated temperature. *ASCE Journal of Materials in Civil Engineering, 34(2),* 4021415.
9. Li, L., Cao, M., Li, Z., Zhang, W., Shi, D. et al. (2022). Uniaxial tensile behavior and mechanism characterization of multi-scale fiber-reinforced cementitious materials. *Materiales de Construcción, 72(345),* e271.
10. Li, L., Li, Z., Cao, M., Tang, Y., Zhang, Z. (2021). Nanoindentation and porosity fractal dimension of calcium carbonate whisker reinforced cement paste after elevated temperatures (up to 900°C). *Fractals, 29(2),* 2140001.
11. Ming, X., Cao, M., Li, L., Yin, H. (2021). Self-healing properties of thermally damaged cement blends. *ACI Materials Journal, 118(2),* 161–172.
12. Li, L., Khan, M., Bai, C., Shi, K. (2021). Uniaxial tensile behavior, flexural properties, empirical calculation and microstructure of multi-scale fiber reinforced cement-based material at elevated temperature. *Materials, 14(8),* 1827.
13. Feng, H., Zhao, X., Li, L., Zhao, X., Gao, D. (2021). Water stability of bonding properties between nano-Fe_2O_3-modified magnesium-phosphate-cement mortar and steel fibre. *Construction and Building Materials, 291,* 123316.
14. Li, Y., Li, L., Bindiganavil, V. (2021). Constitutive model of uniaxial compressive behavior for roller-compacted concrete using coal bottom ash entirely as fine aggregate. *Buildings, 11(5),* 191.
15. Li, L., Guan, J., Xie, Y., Cao, M. (2022). Characterization of bending performance of reinforced cementitious composites beams with hybrid fibers after exposure to high temperatures. *Structural Concrete, 23(1),* 395–411.
16. Li, L., Gao, D., Li, Z., Cao, M., Gao, J. et al. (2020). Effect of high temperature on morphologies of fibers and mechanical properties of multi-scale fiber reinforced cement-based composites. *Construction and Building Materials, 261,* 120487.
17. Ming, X., Cao, M., Lv, X., Yin, H., Li, L. et al. (2020). Effects of high temperature and post-fire-curing on compressive strength and microstructure of calcium carbonate whisker-fly ash-cement system. *Construction and Building Materials, 244,* 118333.
18. Si, W., Cao, M., Li, L. (2020). Establishment of fiber factor for rheological and mechanical performance of polyvinyl alcohol (PVA) fiber reinforced mortar. *Construction and Building Materials, 265,* 120347.
19. Li, L., Cao, M., Xie, C., Yin, H. (2019). Effects of $CaCO_3$ whisker, hybrid fiber content and size on uniaxial compressive behavior of cementitious composites. *Structural Concrete, 20(1),* 506–518.

20. Cao, M., Ming, X., He, K., Li, L., Shen, S. (2019). Effect of macro-, micro- and nano-calcium carbonate on properties of cementitious composites–A review. *Materials, 12(5),* 781.
21. Cao, M., Li, L., Yin, H., Ming, X. (2019). Microstructure and strength of calcium carbonate ($CaCO_3$) whisker reinforced cement paste after exposed to high temperatures. *Fire Technology, 55(6),* 1983–2003.
22. Li, L., Cao, M., Yin, H. (2019). Comparative roles between aragonite and calcite calcium carbonate whiskers in the hydration and strength of cement paste. *Cement and Concrete Composites, 104,* 103350.
23. Li, L., Cao, M., Ming, X., Yin, H., Sun, Y. (2019). Microstructure of calcium carbonate whisker reinforced cement paste after elevated temperature exposure. *Construction and Building Materials, 227,* 116609.
24. Cao, M., Li, L., Shen, S. (2019). Influence of reinforcing index on rheology of fiber-reinforced mortar. *ACI Materials Journal, 116(6),* 95–105.
25. Cao, M., Xie, C., Li, L., Khan, M. (2019). Effect of different PVA and steel fiber length and content on mechanical properties of $CaCO_3$ whisker reinforced cementitious composites. *Materiales de Construcción, 69(336),* 200.
26. Cao, M., Li, L., Zhang, C., Feng, J. (2018). Behaviour and damage assessment of a new hybrid-fibre-reinforced mortar under impact load. *Magazine of Concrete Research, 70(17),* 905–918.
27. Cao, M., Li, L., Khan, M. (2018). Effect of hybrid fibers, calcium carbonate whisker and coarse sand on mechanical properties of cement-based composites. *Materiales de Construcción, 68(330),* e156.
28. Cao, M., Li, L. (2018). New models for predicting workability and toughness of hybrid fiber reinforced cement-based composites. *Construction and Building Materials, 176,* 618–628. DOI 10.1016/j.conbuildmat.2018.05.075.
29. Li, L., Cao, M. (2018). Influence of calcium carbonate whisker and polyvinyl alcohol- steel hybrid fiber on ultrasonic velocity and resonant frequency of cementitious composites. *Construction and Building Materials, 188,* 737–746. DOI 10.1016/j.conbuildmat.2018.08.154.
30. Cao, M., Xie, C., Li, L., Khan, M. (2018). The relationship between reinforcing index and flexural parameters of new hybrid fiber reinforced slab. *Computers and Concrete, 22(5),* 481–492.
31. Li, L., Cao, M. (2018). A new multi-scale hybrid fiber reinforced cement-based composites. *Fibre Reinforced Concrete: From Design to Structural Applications*, pp. 12–19. Lake Garda, Italy.
32. Cao, M., Li, L., Xu, L. (2017). Relations between rheological and mechanical properties of fiber reinforced mortar. *Computers and Concrete, 20(4),* 449–459.
33. Zeng, D., Cao, M. (2022). The flexural behaviors and mechanism of wollastonite microfiber modified ultra-high performance concrete with steel fiber from micro to macro scale. *Archives of Civil and Mechanical Engineering, 22(1),* 32. DOI 10.1007/s43452-021-00340-1.
34. Esmaeili, J., Andalibi, K., Gencel, O., Maleki, F. K., Maleki, V. A. (2021). Pull-out and bond-slip performance of steel fibers with various ends shapes embedded in polymer-modified concrete. *Construction and Building Materials, 271,* 121531. DOI 10.1016/j.conbuildmat.2020.121531.
35. Fan, L., Meng, W., Teng, L., Khayat, K. H. (2020). Effects of lightweight sand and steel fiber contents on the corrosion performance of steel rebar embedded in UHPC. *Construction and Building Materials, 238,* 117709. DOI 10.1016/j.conbuildmat.2019.117709.
36. Zhang, Y., Ju, J. W., Chen, Q., Yan, Z., Zhu, H. et al. (2020). Characterizing and analyzing the residual interfacial behavior of steel fibers embedded into cement-based matrices after exposure to high temperatures. *Composites Part B: Engineering, 191,* 107933. DOI 10.1016/j.compositesb.2020.107933.
37. Patnaik, B., Bhojaraju, C., Mousavi, S. S. (2020). Experimental study on residual properties of thermally damaged steel fiber-reinforced concrete containing copper slag as fine aggregate. *Journal of Material Cycles and Waste Management, 22(3),* 801–815. DOI 10.1007/s10163-020-00972-0.
38. Mo, Y., Pang, J., Huang, J. (2019). Dynamic mechanical properties and fractal characteristics of polypropylene fiber-reinforced cement soil under impact loading. *Advances in Materials Science and Engineering, 2019(5),* 3735891. DOI 10.1155/2019/3735891.
39. Niu, D., Huang, D., Zheng, H., Su, L., Fu, Q. et al. (2019). Experimental study on mechanical properties and fractal dimension of pore structure of basalt-polypropylene fiber-reinforced concrete. *Applied Sciences, 9(8),* 1602. DOI 10.3390/app9081602.

40. Fu, Q., Niu, D., Zhang, J., Huang, D., Hong, M. (2018). Impact response of concrete reinforced with hybrid basalt-polypropylene fibers. *Powder Technology, 326,* 411–424. DOI 10.1016/j.powtec.2017.12.022.
41. Pakravan, H., Jamshidi, M., Latifi, M. (2016). The effect of hybridization and geometry of polypropylene fibers on engineered cementitious composites reinforced by polyvinyl alcohol fibers. *Journal of Composite Materials, 50(8),* 1007–1020. DOI 10.1177/0021998315586078.
42. Tanyildizi, H., Yonar, Y. (2016). Mechanical properties of geopolymer concrete containing polyvinyl alcohol fiber exposed to high temperature. *Construction and Building Materials, 126,* 381–387. DOI 10.1016/j.conbuildmat.2016.09.001.
43. Said, S. H., Razak, H. A., Othman, I. (2015). Flexural behavior of engineered cementitious composite (ECC) slabs with polyvinyl alcohol fibers. *Construction and Building Materials, 75,* 176–188. DOI 10.1016/j.conbuildmat.2014.10.036.
44. Zhang, J., Leng, B. (2008). Transition from multiple macro-cracking to multiple micro-cracking in cementitious composites. *Tsinghua Science & Technology, 13(5),* 669–673. DOI 10.1016/S1007-0214(08)70109-3.
45. Meng, Z., Li, L., Farooqi, M. U., Feng, L., Wang, L. (2021). Fiber factor for fresh and hardened properties of polyethylene fiber-reinforced geopolymer mortar. *Journal of Building Engineering, 53,* 104556. DOI 10.1016/j.jobe.2022.104556.
46. Cao, M., Khan, M. (2021). Effectiveness of multiscale hybrid fiber reinforced cementitious composites under single degree of freedom hydraulic shaking table. *Structural Concrete, 22(1),* 535–549. DOI 10.1002/suco.201900228.
47. Xie, C., Cao, M., Khan, M., Yin, H., Guan, J. (2021). Review on different testing methods and factors affecting fracture properties of fiber reinforced cementitious composites. *Construction and Building Materials, 273,* 121766. DOI 10.1016/j.conbuildmat.2020.121766.
48. Khan, M., Cao, M., Xie, C., Ali, M. (2021). Experimental and analytical study of hybrid fiber reinforced concrete prepared with basalt fiber under high temperature. *Fire and Materials, 46(1),* 205–226.
49. Pu, B., Liu, B., Li, L., Pang, W., Wan, Z. (2020). Influence of polypropylene fibre factor on flowability and mechanical properties of self-compacting geopolymer. *Materials, 14(17),* 5025. DOI 10.3390/ma14175025.
50. Arshad, S., Sharif, M. B., Irfan-ul-Hassan, M., Khan, M., Zhang, J. (2020). Efficiency of supplementary cementitious materials and natural fiber on mechanical performance of concrete. *Arabian Journal for Science and Engineering, 45(10),* 8577–8589. DOI 10.1007/s13369-020-04769-z.
51. Cao, M., Khan, M., Ahmed, S. (2020). Effectiveness of calcium carbonate whisker in cementitious composites. *Periodica Polytechnica Civil Engineering, 64(1),* 265–275. DOI 10.3311/PPci.14288.
52. Khan, M., Cao, M., Ali, M. (2020). Cracking behaviour and constitutive modelling of hybrid fibre reinforced concrete. *Journal of Building Engineering, 30,* 101272. DOI 10.1016/j.jobe.2020.101272.
53. Saulat, H., Cao, M., Khan, M. M., Khan, M., Khan, M. M. et al. (2020). Preparation and applications of calcium carbonate whisker with a special focus on construction materials. *Construction and Building Materials, 236,* 117613. DOI 10.1016/j.conbuildmat.2019.117613.
54. Khan, M., Ali, M. (2019). Improvement in concrete behavior with fly ash, silica-fume and coconut fibres. *Construction and Building Materials, 203,* 174–187. DOI 10.1016/j.conbuildmat.2019.01.103.
55. Khan, M., Ali, M. (2018). Effectiveness of hair and wave polypropylene fibers for concrete roads. *Construction and Building Materials, 166,* 581–591. DOI 10.1016/j.conbuildmat.2018.01.167.
56. Khan, M., Ali, M. (2018). Effect of super plasticizer on the properties of medium strength concrete prepared with coconut fiber. *Construction and Building Materials, 182,* 703–715. DOI 10.1016/j.conbuildmat.2018.06.150.
57. Khan, M., Ali, M. (2016). Use of glass and nylon fibers in concrete for controlling early age micro cracking in bridge decks. *Construction and Building Materials, 125,* 800–808. DOI 10.1016/j.conbuildmat.2016.08.111.
58. Pakravan, H. R., Latifi, M., Jamshidi, M. (2017). Hybrid short fiber reinforcement system in concrete: A review. *Construction and Building Materials, 142,* 280–294. DOI 10.1016/j.conbuildmat.2017.03.059.
59. Pakravan, H. R., Ozbakkaloglu, T. (2019). Synthetic fibers for cementitious composites: A critical and in-depth review of recent advances. *Construction and Building Materials, 207,* 491–518. DOI 10.1016/j.conbuildmat.2019.02.078.

60. Pan, Z., Zhu, Y., Qiao, Z., Meng, S. (2020). Seismic behavior of composite columns with steel reinforced ECC permanent formwork and infilled concrete. *Engineering Structures, 212,* 110541. DOI 10.1016/j.engstruct.2020.110541.
61. Li, V. C., Bos, F. P., Yu, K., McGee, W., Ng, T. Y. et al. (2020). On the emergence of 3D printable engineered, strain hardening cementitious composites (ECC/SHCC). *Cement and Concrete Research, 132,* 106038. DOI 10.1016/j.cemconres.2020.106038.
62. Wang, Q., Yi, Y., Ma, G., Luo, H. (2019). Hybrid effects of steel fibers, basalt fibers and calcium sulfate on mechanical performance of PVA-ECC containing high-volume fly ash. *Cement and Concrete Composites, 97,* 357–368. DOI 10.1016/j.cemconcomp.2019.01.009.
63. Kim, D. J., Park, S. H., Ryu, G. S., Koh, K. T. (2011). Comparative flexural behavior of hybrid ultra high performance fiber reinforced concrete with different macro fibers. *Construction and Building Materials, 25(11),* 4144–4155. DOI 10.1016/j.conbuildmat.2011.04.051.
64. Swamy, R. N., Mangat, P. S. (1974). Influence of fibre-aggregate interaction on some properties of steel fibre reinforced concrete. *Materials and Structures, 7(5),* 307–314.
65. Said, S. H., Razak, H. A. (2015). The effect of synthetic polyethylene fiber on the strain hardening behavior of engineered cementitious composite (ECC). *Materials & Design, 86,* 447–457. DOI 10.1016/j.matdes.2015.07.125.
66. Mehdipour, I., Libre, N. A., Shekarchi, M., Khanjani, M. (2013). Effect of workability characteristics on the hardened performance of FRSCCMs. *Construction and Building Materials, 40,* 611–621. DOI 10.1016/j.conbuildmat.2012.11.051.
67. Emdadi, A., Mehdipour, I., Libre, N. A., Shekarchi, M. (2015). Optimized workability and mechanical properties of FRCM by using fiber factor approach: theoretical and experimental study. *Materials and Structures, 48(4),* 1149–1161. DOI 10.1617/s11527-013-0221-3.
68. Cao, M., Si, W., Xie, C. (2020). Relationship of rheology, fiber dispersion, and strengths of polyvinyl alcohol fiber-reinforced cementitious composites. *ACI Materials Journal, 117(3),* 191–204.
69. ASTM (2016). Standard test method for pulse velocity through concrete (ASTM C597−16): ASTM C597−16. West Conshohocken, PA, USA: ASTM.
70. Bureau of Quality and Technical Supervision of the People's Republic of China (1999). Test method of cement mortar strength (ISO method). Beijing, China: Standards Press of China.
71. Mehdipour, I., Vahdani, M., Libre, N. A., Shekarchi, M. (2013). Relationship between workability and mechanical properties of fibre-reinforced self-consolidating mortar. *Magazine of Concrete Research, 65(17),* 1011–1022. DOI 10.1680/macr.12.00088.
72. Krieger, I. M., Dougherty, T. J. (1959). A mechanism for non-newtonian flow in suspensions of rigid spheres. *Transactions of the Society of Rheology, 3(1),* 137–152. DOI 10.1122/1.548848.
73. Philipse, A. P. (1996). The random contact equation and its implications for (colloidal) rods in packings, suspensions, and anisotropic powders. *Langmuir, 12(5),* 1127–1133. DOI 10.1021/la950671o.
74. Martinie, L., Rossi, P., Roussel, N. (2010). Rheology of fiber reinforced cementitious materials: Classification and prediction. *Cement and Concrete Research, 40(2),* 226–234. DOI 10.1016/j.cemconres.2009.08.032.
75. Aydın, S., Baradan, B. (2013). The effect of fiber properties on high performance alkali-activated slag/silica fume mortars. *Composites Part B: Engineering, 45(1),* 63–69. DOI 10.1016/j.compositesb.2012.09.080.
76. Shi, C., Xie, P. (1998). Interface between cement paste and quartz sand in alkali-activated slag mortars. *Cement and Concrete Research, 28(6),* 887–896. DOI 10.1016/S0008-8846(98)00050-7.
77. Cao, M., Zhang, C., Li, Y., Wei, J. (2015). Using calcium carbonate whisker in hybrid fiber-reinforced cementitious composites. *Journal of Materials in Civil Engineering, 27(4),* 4014139. DOI 10.1061/(ASCE)MT.1943-5533.0001041.
78. Ding, Y., Dai, J., Shi, C. (2018). Fracture properties of alkali-activated slag and ordinary Portland cement concrete and mortar. *Construction and Building Materials, 165,* 310–320. DOI 10.1016/j.conbuildmat.2017.12.202.
79. Cao, M., Zhang, C., Lv, H. (2014). Mechanical response and shrinkage performance of cementitious composites with a new fiber hybridization. *Construction and Building Materials, 57,* 45–52. DOI 10.1016/j.conbuildmat.2014.01.088.